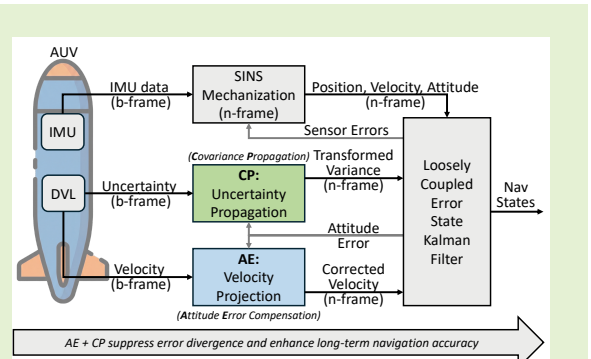


A DVL Aided Loosely Coupled Inertial Navigation Strategy for AUVs with Attitude Error Modeling and Variance Propagation

Jin Huang, Zichen Liu, Haoda Li, Zhikun Wang, and Ying Chen

Abstract—In underwater navigation systems, strap-down inertial navigation system/Doppler velocity log (SINS/DVL)-based loosely coupled architectures are widely adopted. Conventional approaches project DVL velocities from the body coordinate system to the navigation coordinate system using SINS-derived attitude; however, accumulated attitude estimation errors introduce biases into velocity projection and degrade navigation performance during long-term operation. To address this issue, two complementary improvements are introduced. First, a vehicle attitude error-aware DVL velocity transformation model is formulated by incorporating attitude error terms into the observation equation to reduce projection-induced velocity bias. Second, a covariance matrix-based variance propagation method is developed to transform DVL measurement uncertainty across coordinate systems, introducing an expectation-based attitude error compensation term to achieve statistically consistent noise modeling. Simulation and field experiment results demonstrate that both improvements individually enhance navigation accuracy and confirm that accumulated attitude errors affect both projected velocity measurements and their associated uncertainty. When jointly applied, long-term error divergence is effectively suppressed. Field experimental results show that the proposed approach achieves a 78.3% improvement in 3D position RMSE and a 71.8% reduction in the maximum component-wise position error compared with the baseline IMU+DVL method, providing a robust solution for improving long-term SINS/DVL navigation performance.

Index Terms—SINS/DVL, Loosely Coupled, Underwater Navigation, Vehicle Attitude Error, Variance Propagation



I. INTRODUCTION

The ocean has played a crucial role in the course of human development. How to better explore, utilize, and protect the ocean has long been a central goal of humanity's efforts. For much of history, most ocean-related research has focused on the sea surface, employing methods such as aerial surveys and ship-based observations [1], [2]. With advances in science and technology, humanity has gained an increasing number of tools for studying and monitoring the ocean, among which robotic systems have found widespread application [3].

In recent years, both autonomous and unmanned surface and underwater vehicles have become indispensable in a broad spectrum of maritime applications, ranging from large-scale environmental monitoring and climate change mitigation to the protection, inspection, and surveillance of critical seabed infrastructure against sabotage, accidental damage, or unauthorized activities [4]. This growing operational landscape underscores the strategic importance of reliable navigation and positioning technologies, particularly for autonomous platforms operating in complex and dynamic marine environments [5].

As a prominent representative of such systems, the autonomous underwater vehicles (AUVs) have garnered significant attention in research due to their vast potential in underwater exploration, scientific studies, and monitoring applications [6], [7]. However, because of the rapid attenuation of electromagnetic waves, traditional navigation methods, such as the global navigation satellite system (GNSS), are not applicable in underwater environments [8]. As a result, the navigation and positioning of underwater vehicles continue to present substantial challenges [9]. Therefore, the accuracy of the navigation system is critical for the successful operation of AUVs. Currently, traditional underwater navigation systems include the strap-down inertial navigation system (SINS), Doppler velocity log (DVL), and ultra-short baseline positioning system (USBL), among others [10], [11].

Due to the control requirements of underwater vehicles, high-precision position, velocity, and attitude information is essential [12]. As a result, integrated navigation systems (INS)

Corresponding author: Zhikun Wang and Ying Chen.

Jin Huang, Zichen Liu, Haoda Li, and Ying Chen are with the State Key Laboratory of Ocean Sensing, Ocean College of Zhejiang University, Zhoushan, 316021, China (e-mail: jin.huang, zichen.liu, haodleo, ychen@zju.edu.cn).

Zhikun Wang is with the Donghai Laboratory, Zhoushan, 316021, China (e-mail: wang.zk@zju.edu.cn).

centered around SINS have been widely applied in underwater environments. However, since SINS fundamentally relies on the integration of outputs from the inertial measurement unit (IMU), errors accumulate over time, leading to divergence in navigation results [13]. To mitigate this issue, external observations are often introduced as constraints to suppress error divergence. In practical applications, DVL provides high-precision velocity measurements, and due to its easy installation and strong concealability, it is widely used in integrated navigation systems to constrain SINS error divergence and provide high-quality navigation data [14].

Currently, most commonly available DVL devices output the three-axis velocity corresponding to the DVL's body coordinate system. A few devices equipped with a magnetic compass and attitude sensors can provide velocity information in the northward, eastward, and downward directions. However, due to the presence of devices such as the magnetic compass, DVL velocity measurements are highly susceptible to interference, which, in turn, affects the stability of the navigation system [15], [16]. Therefore, in most studies, DVLs that output velocity in the body coordinate system are used as velocity observations.

In loosely coupled integrated navigation systems, the DVL velocity measurement is transformed into the navigation frame (n -frame), and the observation equation is subsequently constructed in the n -frame. The most common method is to convert the DVL velocity measurement using the INS attitude output, which assumes that the vehicle's attitude must be accurate. However, in practice, the vehicle's attitude is often inaccurate and tends to accumulate over time during navigation, introducing errors into the DVL velocity measurement. For simplicity, most studies assume that the vehicle's attitude is accurate and only consider the DVL installation offset angle and lever arm relative to the SINS coordinate system [17].

Some researchers have studied the impact of the vehicle's attitude on DVL velocity measurements, focusing primarily on how the vehicle's position and instantaneous angular velocity affect the reception of DVL signals [18]. Due to changes in the vehicle's attitude, the DVL velocity measurement is affected. Researchers have introduced attitude measuring instruments to compensate for errors in the DVL beam velocity [19], [20]. Some researchers have recognized the impact of attitude errors on DVL velocity transformation and have implemented simple compensations for these errors [21]. However, they have overlooked the influence of factors such as lever arm errors [22], [23].

In tightly integrated navigation systems, researchers convert the INS velocity to the DVL body coordinate system and then construct the observation equation in the body frame (b -frame). Most studies assume that the vehicle's attitude is accurate and only consider the DVL installation offset angle and lever arm relative to the SINS coordinate system [24]. Additionally, some researchers have assumed that attitude errors have no impact when converting the INS velocity to the body coordinate system [25], [26].

Furthermore, as an important external sensor, the error metrics output by the DVL are critical parameters. These error parameters play a significant role in assessing the uncertainty

of velocity measurements, constructing the measurement noise covariance matrix, and adjusting filter gains [27]. In a loosely coupled integrated navigation system, since the DVL observations need to be projected from the b -frame to the n -frame, the corresponding errors in the b -frame must also be projected into the new coordinate system. However, the standard deviation vector output by the DVL cannot be directly transformed using the direction cosine matrix (DCM), and this issue has rarely been addressed in the literature [28].

In summary, previous studies have primarily focused on the misalignment between the DVL coordinate system and the vehicle body frame, treating this Euclidean-space error as a constant parameter to be estimated. Since the DVL is typically rigidly mounted on the vehicle, such installation-related misalignment can be calibrated once and subsequently reused. However, in a practical SINS/DVL loosely coupled navigation system, the DVL velocity measurements must be further projected from the body frame into the navigation frame to construct the velocity observation equation. This projection process inevitably introduces errors associated with vehicle attitude estimation, which are generally time-varying and accumulate during long-term operation. As a result, attitude estimation errors of the vehicle lead to biased velocity projections, thereby degrading the reliability of DVL-based velocity observations, especially in high-dynamic underwater environments and long-duration missions. Despite its practical significance, this issue has received limited attention in existing literature, where attitude errors are often neglected or considered independently from the velocity transformation process.

To address these limitations, this paper reconstructs a SINS/DVL loosely coupled navigation framework that explicitly accounts for vehicle attitude errors in the DVL velocity projection. By incorporating attitude error terms into the DVL observation equation, a more accurate velocity mapping from the body frame to the navigation frame is achieved. Furthermore, to properly model the propagation of DVL measurement uncertainty during this transformation, an expectation-based attitude error compensation term is derived. Considering the non-rotatable nature of standard deviation vectors, a covariance matrix-based variance propagation method is introduced to ensure statistically consistent uncertainty transformation across coordinate systems. Through the combined treatment of attitude error-aware velocity projection and covariance-based uncertainty propagation, the proposed approach effectively compensates for DVL observation degradation caused by vehicle attitude uncertainty, thereby enhancing the long-term navigation performance and robustness of SINS/DVL loosely coupled systems.

The main contributions of this article are summarized as follows.

1. A vehicle attitude error-aware DVL velocity transformation model is established for SINS/DVL loosely coupled navigation systems. By explicitly incorporating vehicle attitude errors into the DVL observation equation, the proposed model enables more accurate velocity projection from the body coordinate system to the navigation coordinate system and mitigates velocity biases caused by

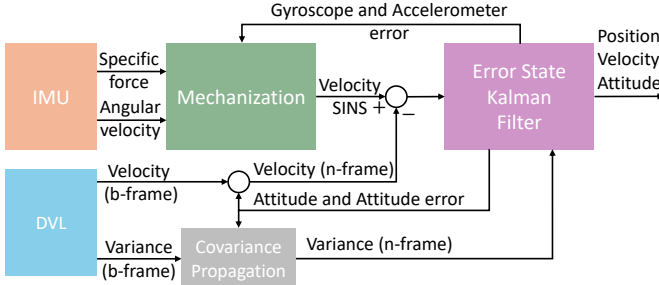


Fig. 1. SINS/DVL system framework in this paper.

accumulated attitude estimation errors during long-term operation.

2. To address the inconsistency of directly transforming DVL measurement variance across coordinate systems, a covariance matrix-based variance propagation method is proposed. This method employs the covariance matrix as an intermediate representation and introduces an expectation-based attitude error compensation term, thereby achieving a statistically consistent transformation of DVL measurement uncertainty from the body frame to the navigation frame.
3. The effectiveness of the proposed methods is comprehensively validated through simulations and field experiments. Experimental results demonstrate that each method individually mitigates navigation errors and improves overall accuracy. Moreover, when both methods are jointly applied, the RMSE position error magnitude is reduced by 78.3%, and the maximum component-wise position error is decreased by 71.8%, compared with the baseline IMU+DVL approach.

The structure of this paper is organized as follows: Section II provides a brief introduction to the SINS/DVL integrated navigation system. Section III presents the proposed SINS/DVL integrated navigation method, which accounts for vehicle attitude errors and variance propagation. Section IV discusses the simulation and experimental results, with the simulation results presented in subsection IV-A, the field experimental results in subsection IV-B, and an analysis of the results in subsection IV-C. Finally, the conclusions are presented in Section V.

II. BRIEF REVIEW OF SINS/DVL INTEGRATED NAVIGATION SYSTEM

A. System Structure

The SINS/DVL system consists of an IMU and a DVL, as shown in Fig. 1. The IMU includes a triaxial gyroscope and a triaxial accelerometer, which are used to measure the vehicle's angular velocity and acceleration, respectively. The DVL measures the velocity of the vehicle in the body frame.

The system model of the loosely coupled SINS/DVL integrated navigation system is expressed as follows:

$$\begin{cases} \dot{\mathbf{X}} = \mathbf{F}\mathbf{X} + \mathbf{G}\mathbf{W} \\ \mathbf{Z} = \mathbf{H}\mathbf{X} + \mathbf{N} \end{cases} \quad (1)$$

In the state transition equation, \mathbf{Z} represents the observation vector, \mathbf{F} is the system dynamics matrix, \mathbf{G} is the noise distribution matrix, and \mathbf{W} is the process noise vector, as described in [29], [30]. In the observation equation, \mathbf{X} is the state vector, \mathbf{H} is the observation matrix, and \mathbf{N} is the measurement noise vector.

The 21-dimension state vector \mathbf{X} is defined as:

$$\mathbf{X} = \begin{bmatrix} (\delta\mathbf{r}^n)^\top & (\delta\mathbf{v}^n)^\top & \phi^\top & \mathbf{b}_g^\top & \mathbf{b}_a^\top & \mathbf{s}_g^\top & \mathbf{s}_a^\top \end{bmatrix}^\top \quad (2)$$

where $\delta\mathbf{r}^n$ and $\delta\mathbf{v}^n$ represent the position and velocity errors in the n -frame, ϕ denotes the attitude error, \mathbf{b}_g and \mathbf{b}_a represent the gyroscope and accelerometer bias errors, and \mathbf{s}_g and \mathbf{s}_a are the scale factor errors of the gyroscope and accelerometer, respectively.

The measurement vector \mathbf{Z} corresponds to the velocity difference between the DVL and SINS, and can be expressed as follows:

$$\mathbf{Z} = \hat{\mathbf{v}}_{\text{DVL}}^n - \tilde{\mathbf{v}}_{\text{DVL}}^n \quad (3)$$

where $\hat{\mathbf{v}}_{\text{DVL}}^n$ represents the velocity of the DVL phase center, as estimated by the INS, and $\tilde{\mathbf{v}}_{\text{DVL}}^n$ denotes the velocity measured by the DVL, which is transformed from the b -frame.

III. PROPOSED SINS/DVL INTEGRATED METHOD CONSIDERING VEHICLE'S ATTITUDE

Currently, most studies primarily assume that the vehicle's attitude is accurate or only model the impact of attitude errors in a simplified manner. Furthermore, few studies address the propagation of DVL velocity variance in this process. Therefore, this section investigates the DVL observation update, considering vehicle attitude errors, along with the corresponding variance propagation process based on the covariance matrix. For simplicity, the IMU mentioned hereafter will refer to the SINS system, and in the equations, it will represent the measurements from the SINS system at the IMU's reference center.

A. DVL Measurement Equation Considering Vehicle's Attitude Error

Before defining the measurement equation, the error model of the DVL should be analyzed. In this paper, we assume that the DVL installation offset angle and lever arm relative to the INS coordinate system can be precisely calibrated [31]. The DVL measures the velocity of the vehicle in the b -frame, which can be expressed as:

$$\mathbf{v}_{\text{DVL}}^b = [v_x^b \ v_y^b \ v_z^b]^\top \quad (4)$$

where v_x^b , v_y^b , and v_z^b are the velocities corresponding to the axes of the Front-Right-Bottom body frame coordinate, respectively.

As mentioned in formula (2), the velocity state is defined in the navigation frame, meaning that the DVL velocity measurement must be transformed into the n -frame. In most studies, the DVL velocity transformation assumes the vehicle's attitude is accurate. However, in practice, the vehicle's attitude

is not always precise, which introduces errors into the DVL velocity measurement. Therefore, the DVL velocity measurement should be transformed into the n -frame while accounting for the vehicle's attitude error.

Taking the vehicle's attitude error into account, the DVL velocity measurement can be transformed into the n -frame as follows:

$$\mathbf{v}_{\text{DVL}}^n = \hat{\mathbf{C}}_b^n \mathbf{v}_{\text{DVL}}^b = \mathbf{C}_n^{n'} \mathbf{C}_b^n \mathbf{v}_{\text{DVL}}^b \quad (5)$$

where $\mathbf{C}_n^{n'}$ is the direction cosine matrix from the true n' -frame to the SINS-calculated n -frame, and $\hat{\mathbf{C}}_b^n$ is the DCM from the SINS-calculated n -frame to the b -frame. Considering that the vehicle's attitude error is a small angular error, it can be approximated as:

$$\hat{\mathbf{C}}_b^n = \mathbf{C}_n^{n'} \mathbf{C}_b^n = [\mathbf{I} - (\phi \times)] \mathbf{C}_b^n \quad (6)$$

where \mathbf{I} is the identity matrix, and ϕ represents the attitude error. The operator $(\cdot \times)$ denotes the skew-symmetric matrix.

Assuming no other errors are present, due to the existence of the DVL's lever arm \mathbf{l}^b , the velocity measured by the IMU and the velocity measured by the DVL can be related as follows

$$\mathbf{v}_{\text{IMU}}^n = \mathbf{v}_{\text{DVL}}^n + (\omega_{in}^n \times) \mathbf{C}_b^n \mathbf{l}^b + \mathbf{C}_b^n (\mathbf{l}^b \times \omega_{ib}^b) \quad (7)$$

where $\mathbf{v}_{\text{IMU}}^n$ is the velocity vector in the IMU navigation frame, ω_{in}^n is the projection of the angular velocity vector of the n -frame onto the inertial frame (i -frame) in the n -frame, and ω_{ib}^b is the gyroscope output in the b -frame.

The error perturbation is defined as follows:

$$\begin{cases} \hat{\mathbf{v}}_{\text{IMU}}^n = \mathbf{v}_{\text{IMU}}^n + \delta \mathbf{v}^n \\ \hat{\mathbf{v}}_{\text{DVL}}^b = \mathbf{v}_{\text{DVL}}^b - \mathbf{n}_v^b \\ \hat{\omega}_{ib}^b = \omega_{ib}^b + \delta \omega_{ib}^b \\ \delta \omega_{ib}^b = b_g + \text{diag}(\omega_{ib}^b) s_g + \omega_\phi \end{cases} \quad (8)$$

where $\delta \mathbf{v}^n$ is the velocity error in the n -frame, \mathbf{n}_v^b is the DVL velocity measurement noise in the b -frame, $\delta \omega_{ib}^b$ is the gyroscope angular velocity measurement error in the b -frame, b_g is the gyroscope bias error, s_g is the gyroscope scale factor error, and ω_ϕ is the gyroscope measurement white noise.

Incorporating formula (8) into formula (7), the estimated value $\hat{\mathbf{v}}_{\text{DVL}}^n$ and the observed value $\tilde{\mathbf{v}}_{\text{DVL}}^n$ of the DVL velocity in the n -frame can be expressed as follows:

$$\begin{aligned} \hat{\mathbf{v}}_{\text{DVL}}^n &= \hat{\mathbf{v}}_{\text{IMU}}^n - (\hat{\omega}_{in}^n \times) \hat{\mathbf{C}}_b^n \mathbf{l}^b - \hat{\mathbf{C}}_b^n (\mathbf{l}^b \times \hat{\omega}_{ib}^b) \\ &= (\mathbf{v}_{\text{IMU}}^n + \delta \mathbf{v}_{\text{IMU}}^n) \\ &\quad - [(\omega_{in}^n \times) + (\delta \omega_{in}^n \times)] [\mathbf{I} - (\phi \times)] \mathbf{C}_b^n \mathbf{l}^b \\ &\quad - [\mathbf{I} - (\phi \times)] \mathbf{C}_b^n (\mathbf{l}^b \times) (\omega_{ib}^b + \delta \omega_{ib}^b) \end{aligned} \quad (9)$$

$$\begin{aligned} \tilde{\mathbf{v}}_{\text{DVL}}^n &= \hat{\mathbf{C}}_b^n \tilde{\mathbf{v}}_{\text{DVL}}^b \\ &= [\mathbf{I} - (\phi \times)] \mathbf{C}_b^n \tilde{\mathbf{v}}_{\text{DVL}}^b \\ &= [\mathbf{I} - (\phi \times)] \mathbf{C}_b^n (\mathbf{v}_{\text{DVL}}^n - \mathbf{C}_b^n \mathbf{n}_v^b) \\ &= \mathbf{C}_b^n \mathbf{v}_{\text{DVL}}^b + \mathbf{C}_b^n \mathbf{n}_v^b - (\phi \times) \mathbf{C}_b^n \mathbf{v}_{\text{DVL}}^b \\ &\quad + (\phi \times) \mathbf{C}_b^n \mathbf{n}_v^b \\ &= \mathbf{v}_{\text{DVL}}^n + \mathbf{C}_b^n \mathbf{n}_v^b - (\phi \times) \mathbf{C}_b^n \mathbf{v}_{\text{DVL}}^b + (\phi \times) \mathbf{C}_b^n \mathbf{n}_v^b \end{aligned} \quad (10)$$

where $\mathbf{v}_{\text{IMU}}^n$ is the velocity vector in the IMU navigation frame.

Considering that the velocity contribution from the motion of the n -frame relative to the i -frame acting on the lever arm is negligible, and that the error in ω_{in}^n can be ignored, Eq. 9 can be further expanded and rearranged as follows:

$$\begin{aligned} \hat{\mathbf{v}}_{\text{DVL}}^n &\approx \hat{\mathbf{v}}_{\text{IMU}}^n - (\omega_{in}^n \times) \mathbf{C}_b^n \mathbf{l}^b - \mathbf{C}_b^n (\mathbf{l}^b \times) \omega_{ib}^b \\ &\quad + (\omega_{in}^n) (\phi \times) \mathbf{C}_b^n \mathbf{l}^b - \mathbf{C}_b^n (\mathbf{l}^b \times) \delta \omega_{ib}^b \\ &\quad + (\phi \times) \mathbf{C}_b^n (\mathbf{l}^b \times) \omega_{ib}^b \\ &\approx \mathbf{v}_{\text{DVL}}^n + (\omega_{in}^n) (\phi \times) \mathbf{C}_b^n \mathbf{l}^b - \mathbf{C}_b^n (\mathbf{l}^b \times) \delta \omega_{ib}^b \\ &\quad + (\phi \times) \mathbf{C}_b^n (\mathbf{l}^b \times) \omega_{ib}^b \end{aligned} \quad (11)$$

The velocity observation vector is expressed as the difference between the velocity estimated by the INS and the velocity measured by the DVL. Substituting the Eq. 10 and Eq. 11 into Eq. 3, and neglecting the second-order terms, we obtain the following:

$$\begin{aligned} \mathbf{Z}_v &= \hat{\mathbf{v}}_{\text{DVL}}^n - \tilde{\mathbf{v}}_{\text{DVL}}^n \\ &\approx (\omega_{in}^n) (\phi \times) \mathbf{C}_b^n \mathbf{l}^b - \mathbf{C}_b^n (\mathbf{l}^b \times) \delta \omega_{ib}^b \\ &\quad + (\phi \times) \mathbf{C}_b^n (\mathbf{l}^b \times) \omega_{ib}^b - \mathbf{C}_b^n \mathbf{n}_v^b + (\phi \times) \mathbf{C}_b^n \mathbf{v}_{\text{DVL}}^b \\ &\quad - (\phi \times) \mathbf{C}_b^n \mathbf{n}_v^b \end{aligned} \quad (12)$$

Overall, the DVL velocity, considering the vehicle's attitude error observation function, can be expressed as follows:

$$\mathbf{Z}_v = \mathbf{H}_v \delta \mathbf{x} + \mathbf{N}_v \quad (13)$$

where the observation matrix \mathbf{H}_v and the measurement noise \mathbf{N}_v are expressed as follows:

$$\begin{cases} \mathbf{H}_v = [\mathbf{0}_3 \quad \mathbf{I}_3 \quad \mathbf{H}_\phi \quad \mathbf{H}_{bg} \quad \mathbf{0}_3 \quad \mathbf{H}_{sg} \quad \mathbf{0}_3] \\ \mathbf{H}_\phi = -(\omega_{in}^n \times) (\mathbf{C}_b^n \mathbf{l}^b \times) \\ \quad - \left\{ \left[\mathbf{C}_b^n (\mathbf{l}^b \times \omega_{in}^n) \right] \times \right\} - \mathbf{C}_b^n \mathbf{v}_{\text{IMU}}^b \\ \mathbf{H}_{bg} = -\mathbf{C}_b^n (\mathbf{l}^b \times) \\ \mathbf{H}_{sg} = -\mathbf{C}_b^n (\mathbf{l}^b \times) \text{diag}(\omega_{ib}^b) \end{cases} \quad (14)$$

$$\mathbf{N}_v = -[\mathbf{I} + (\phi \times)] \mathbf{C}_b^n \mathbf{N}_v^b \quad (15)$$

where $\mathbf{0}_3$ is a 3×3 zero matrix, \mathbf{I}_3 is a 3×3 identity matrix, and $\mathbf{v}_{\text{IMU}}^n$ is the velocity vector in the IMU n -frame.

B. Variance Propagation with Covariance Matrix

In practical applications, the DVL velocity measurement noise is typically characterized by the standard deviation of the velocity measurements, σ_v^b [32]. Most DVL manufacturers provide the standard deviation of the velocity measurements in the b -frame, implying that the measurement noise should be consistently transformed into the n -frame during each measurement update.

It should be emphasized that the standard deviation vector is not a geometric vector. Instead, it describes the dispersion of the measurement components and therefore cannot be directly rotated by a direction cosine matrix in a statistically consistent manner, as shown in (15). To address this issue, this paper introduces the covariance matrix of the observation error as an intermediate variable to represent measurement uncertainty across different coordinate systems. Unlike the standard deviation vector, the covariance matrix captures the second-order statistics of multivariate random variables and can be properly transformed via rotation [27], [33].

The covariance matrix of the DVL velocity measurement noise in the b -frame is constructed as

$$\Sigma_v^b = \text{diag}([\sigma_x^2 \ \sigma_y^2 \ \sigma_z^2]), \quad (16)$$

where σ_x , σ_y , and σ_z are the standard deviations of the velocity measurements along the x , y , and z -axes of the b -frame, respectively.

Given the nominal attitude rotation matrix C_b^n , the corresponding covariance matrix in the n -frame can be obtained using the standard covariance transformation rule:

$$\Sigma_v^n = C_b^n \Sigma_v^b (C_b^n)^\top. \quad (17)$$

However, the above transformation assumes that the attitude is perfectly known. In practice, the attitude estimated by the SINS is uncertain, and this uncertainty affects the mapping of the DVL measurement noise from the b -frame to the n -frame. Using the first-order small-angle attitude error model

$$\hat{C}_b^n \approx [\mathbf{I} - (\phi \times)] C_b^n, \quad (18)$$

the propagated covariance should be interpreted in a stochastic sense. Specifically, rather than requiring the unknown instantaneous value of ϕ , its effect is incorporated through its second-order statistics. Let $P_{\phi\phi} \triangleq \mathbb{E}[\phi\phi^\top]$ denote the attitude error covariance, which can be extracted from the overall state covariance matrix of the integrated navigation system. Define

$$\mathbf{A} \triangleq C_b^n \Sigma_v^b (C_b^n)^\top. \quad (19)$$

Then, the covariance matrix of the DVL velocity measurement noise in the n -frame can be expressed as

$$\Sigma_v^n = \mathbf{A} + \mathbb{E}[(\phi \times) \mathbf{A} (\phi \times)^\top]. \quad (20)$$

By expressing $(\phi \times) = \sum_{i=1}^3 \phi_i \mathbf{S}_i$ with constant basis matrices \mathbf{S}_i , the expectation term in (20) admits the following computable closed form:

$$\mathbb{E}[(\phi \times) \mathbf{A} (\phi \times)^\top] = \sum_{i=1}^3 \sum_{j=1}^3 (P_{\phi\phi})_{ij} \mathbf{S}_i \mathbf{A} \mathbf{S}_j^\top. \quad (21)$$

TABLE I
SIMULATION SPECIFICATIONS

Equipment	Specification	Accuracy
Gyroscope	Constant bias	0.01 deg/h
	Random walk	0.01 deg/√h
	Scale factor error	100 ppm
	Measurement frequency	100 Hz
Accelerometer	Constant bias	50 μg
	Random walk	10 μg/√Hz
	Scale factor error	100 ppm
	Measurement frequency	100 Hz
DVL	Velocity error	1.15%v
	Measurement frequency	2 Hz

After covariance propagation, the measurement noise vector in (15) can be equivalently written as

$$\mathbf{N}_v = \sqrt{\text{diag}(\Sigma_v^n)}. \quad (22)$$

Therefore, the vehicle's attitude error-based navigation (AE) method and covariance propagation navigation (CP) method are proposed in this paper.

IV. RESULT AND DISCUSSION

A. Simulation

In order to fully verify the performance of the proposed AE and CP methods, a simulation experiment is designed.

The entire simulation lasts for 4000 seconds, and the simulation trajectory is shown in Fig. 2, which includes 600 seconds of initial alignment and 3400 seconds for diving, acceleration, deceleration, and coordinated turns. The initial geographic latitude and longitude are 30.0° and 120.0°, respectively, and the initial depth is 0 m. The simulation specifications are shown in Table I.

Fig. 2 shows the simulation trajectory, which illustrates the performance of the integrated navigation system, including the IMU+DVL method, the IMU+DVL method considering vehicle attitude error (AE), the IMU+DVL method using covariance propagation (CP), the IMU+DVL method combining AE and CP, and the ground truth. It is noteworthy that, in the IMU+DVL with the CP method, the covariance matrix uses formula (17) to transform the DVL velocity measurement noise to the n -frame.

Table II reports the root mean square error (RMSE) and maximum values of the simulated position, velocity, and attitude errors. The following discussion examines each error type in detail.

Fig. 3 shows the position error of the integrated navigation system. In the IMU+DVL system, introducing either the AE method or the CP method individually achieves good positioning accuracy. Compared to the unmodified IMU+DVL integrated navigation method, the divergence of the positioning error is effectively suppressed. The RMSE of position errors are: 28.35 m for the IMU+DVL method, 8.14 m for the IMU+DVL method with AE, 9.27 m for the IMU+DVL method with CP, and 7.86 m for the IMU+DVL method combining AE and CP. In terms of maximum positioning error, the results are as follows: 49.44 m for the IMU+DVL method, 16.85 m for the IMU+DVL method with AE, 14.83 m for the

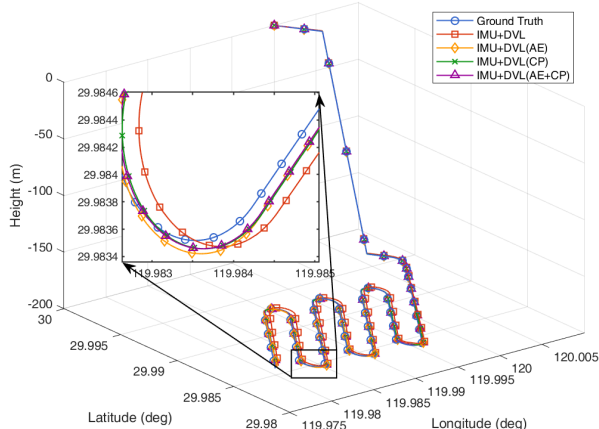


Fig. 2. Simulation trajectory with different methods.

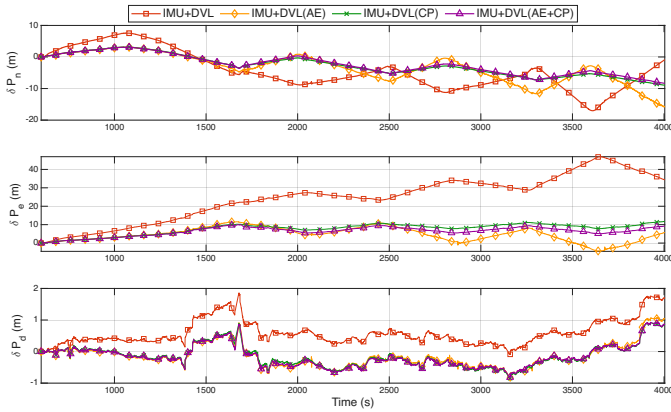


Fig. 3. Position error with IMU+DVL, IMU+DVL (AE), IMU+DVL (CP), and IMU+DVL (AE+CP).

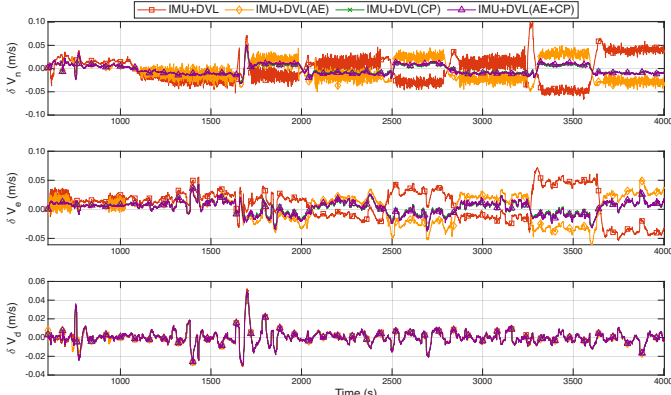


Fig. 4. Velocity error with IMU+DVL, IMU+DVL (AE), IMU+DVL (CP), and IMU+DVL (AE+CP).

IMU+DVL method with CP, and 12.46 m for the IMU+DVL method combining AE and CP.

In summary, the IMU+DVL method combining AE and CP achieves the lowest RMSE while effectively reducing the maximum positioning error.

Fig. 4 and Fig. 5 show the velocity and attitude errors of the integrated navigation system with different methods, respec-

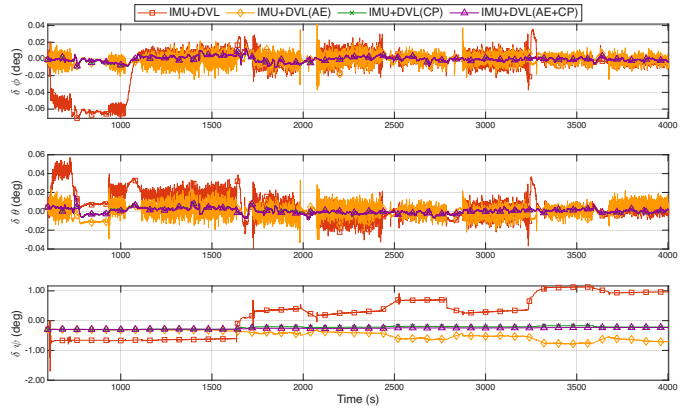


Fig. 5. Attitude error with IMU+DVL, IMU+DVL (AE), IMU+DVL (CP), and IMU+DVL (AE+CP).

TABLE II
THE POSITION, VELOCITY, AND ATTITUDE ERRORS OF THE IMU+DVL, IMU+DVL (AE), IMU+DVL (CP), AND IMU+DVL (AE+CP) METHODS.

Error Type	INS	INS (AE)	INS (CP)	INS (AE+CP)
Pos (m)	RMSE	28.35	8.14	9.27
	Max	49.44	16.85	14.83
Vel (m/s)	RMSE	0.039	0.032	0.017
	Max	0.11	0.075	0.070
Att (deg)	RMSE	0.67	0.50	0.23
	Max	1.70	0.79	0.31

tively. The results demonstrate that the IMU+DVL method with AE and CP can effectively suppress the divergence of both the velocity and attitude errors. The RMSE velocity errors are as follows: 0.039 m/s for the IMU+DVL method, 0.032 m/s for the IMU+DVL method with AE, 0.017 m/s for the IMU+DVL method with CP, and 0.017 m/s for the IMU+DVL method combining AE and CP. The RMSE attitude errors are as follows: 0.67° for the IMU+DVL method, 0.50° for the IMU+DVL method with AE, 0.23° for the IMU+DVL method with CP, and 0.26° for the IMU+DVL method combining AE and CP.

Fig. 6 presents a box plot comparing the position errors of four different methods: IMU+DVL, IMU+DVL (AE), IMU+DVL (CP), and IMU+DVL (AE+CP). It is evident that the IMU+DVL method exhibits the largest position error, with a wide interquartile range (IQR) and significant upper-end outliers. Specifically, its maximum error reaches 49.4435 m, with an IQR of approximately 25 m and no finite outliers. This indicates that the method suffers from high variability and inconsistency, leading to large deviations in positioning accuracy. The result is consistent with Fig. 3, further reinforcing that IMU+DVL alone is insufficient for reliable positioning.

The IMU+DVL (AE) method shows an improvement over IMU+DVL, with a reduced maximum error of 16.8499 m but still a relatively wide IQR of about 8 m. Its box plot reveals a wider IQR and a longer upper whisker. This suggests that while IMU+DVL (AE) reduces the overall error, it introduces higher variability. The presence of extreme values at the upper end indicates that in certain cases, the method produces

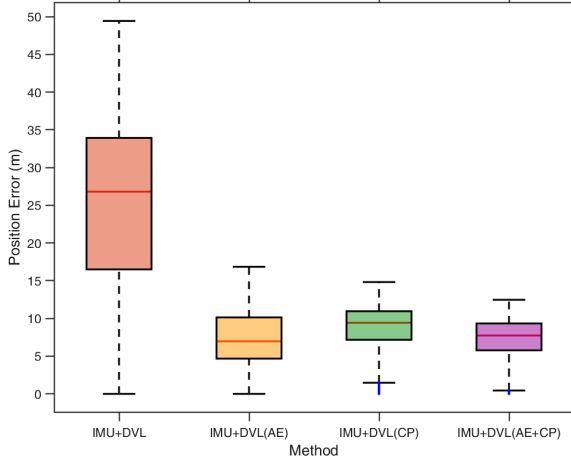


Fig. 6. The box plot of position error with IMU+DVL, IMU+DVL (AE), IMU+DVL (CP), and IMU+DVL (AE+CP).

significantly larger errors, reducing its robustness.

The IMU+DVL (CP) method demonstrates more stable performance compared to IMU+DVL (AE), as indicated by its narrower box and shorter whiskers. Its maximum error is 14.8279 m, with an IQR of roughly 4 m. The reduction in IQR implies that the position errors are more concentrated and less variable. Additionally, the method exhibits fewer outliers, suggesting enhanced stability. Although IMU+DVL (CP) provides a balanced trade-off between accuracy and consistency, it still shows slightly larger upper whiskers, indicating occasional larger errors.

The IMU+DVL (AE+CP) method exhibits the most favorable performance among all four methods. It achieves the lowest maximum error of 12.4688 m, the narrowest IQR of about 3 m. Its box plot has the narrowest IQR, signifying the smallest spread in errors and the highest level of consistency. Furthermore, its outliers appear only at the lower end of the error range, suggesting that in some cases, this method achieves even smaller errors than expected. The RMSE position error for IMU+DVL (AE+CP) is also the lowest among all methods, further confirming its superiority. The absence of significant upper-end outliers and its compact distribution indicate that IMU+DVL (AE+CP) not only reduces error magnitude but also enhances stability, making it the most reliable and robust method for accurate positioning.

B. Field Experiment

The field experiment was conducted in a lake at Zhejiang University to verify the performance of the proposed AE and CP methods in a real-world scenario. The experimental platform is shown in Fig. 7, which includes the SINS/DVL integrated navigation system and the ground truth system (DGNSS). The DGNSS activated the continuous operational reference system (CORS) service, which is capable of providing centimeter-level positioning accuracy for the ground truth. The sensor specifications are shown in Table III.

The entire movement trajectory is shown in Fig. 8. The process lasted 1685 seconds, including 600 seconds of initial

TABLE III FIELD EXPERIMENT SPECIFICATIONS		
Equipment	Specification	Accuracy
Gyroscope	Constant bias	0.03 deg/h
	Random walk	0.005 deg/ \sqrt{h}
	Scale factor error	100 ppm
	Measurement frequency	100 Hz
Accelerometer	Constant bias	300 μ g
	Random walk	0.05 m/s/ \sqrt{h}
	Scale factor error	200 ppm
	Measurement frequency	100 Hz
DVL	Velocity error	1.15%v
DGNSS	Measurement frequency	2 Hz
DGNSS	Position (CORS)	0.02 m

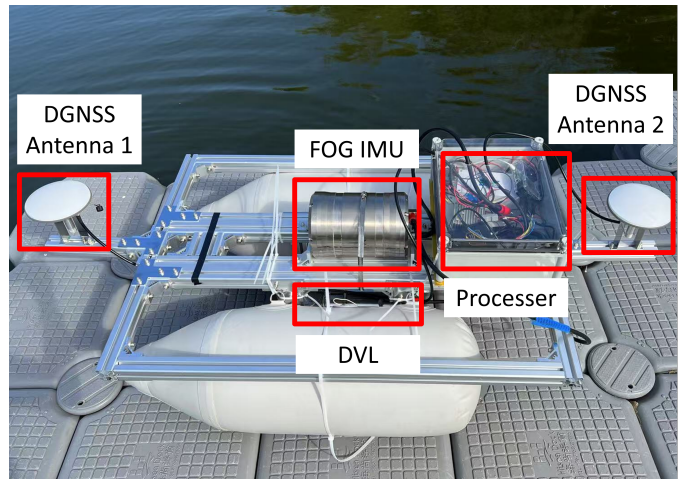


Fig. 7. The surface experiment platform equipped with the SINS/DVL integrated navigation system and the ground truth system (DGNSS).

alignment in a dynamic environment and 1085 seconds of motion in the lake. The IMU+DVL, IMU+DVL (AE), IMU+DVL (CP), and IMU+DVL (AE+CP) methods were also compared in this experiment.

Fig. 9 illustrates the position errors for four different methods. In the navigation coordinate system, along the NED (North, East, Down) directions, the IMU+DVL method exhibits the largest position error, while the IMU+DVL (AE+CP) method demonstrates the smallest position error. In comparison with the IMU+DVL (AE+CP) method, the IMU+DVL (AE) and IMU+DVL (CP) methods show a slight deterioration in positioning accuracy in the northward direction during the later phase of navigation. In the eastward direction, the IMU+DVL (AE+CP) method shows slightly better positioning accuracy than the IMU+DVL (CP) method, while the IMU+DVL (AE) method exhibits relatively larger errors at 1100 seconds. And in the downward direction, the IMU+DVL (CP) and IMU+DVL (AE+CP) methods demonstrate similar accuracy, whereas the IMU+DVL (AE) method shows approximately half the accuracy of the previous two methods in the later stages. The detailed analysis data are listed in Table IV, which summarizes the RMSE and maximum position errors along the N/E/D axes. Overall, the IMU+DVL (AE+CP) method achieves the lowest RMSE and maximum errors among the compared methods.

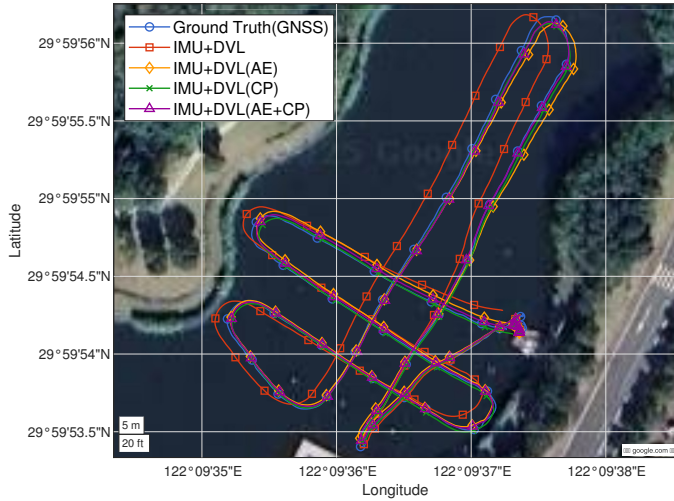


Fig. 8. Experiment trajectory with different methods.

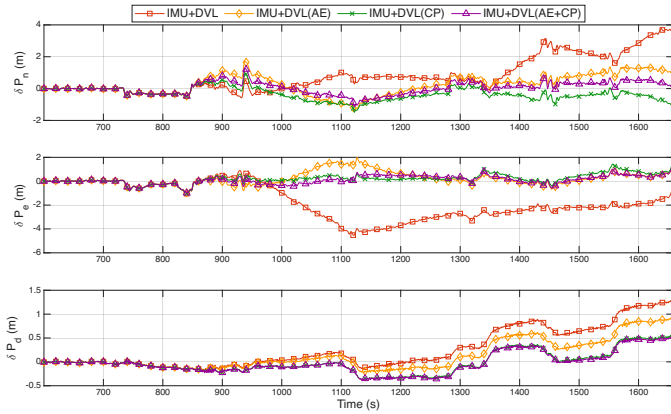


Fig. 9. Position errors from the experimental results using the methods IMU+DVL, IMU+DVL (AE), IMU+DVL (CP), and IMU+DVL (AE+CP).

Fig. 10 presents a box plot comparing the position errors of four different methods: IMU+DVL, IMU+DVL (AE), IMU+DVL (CP), and IMU+DVL (AE+CP), based on experimental data.

The IMU+DVL method exhibits the largest position error, as indicated by the wide IQR and the presence of significant outliers at the upper end. This suggests that the IMU+DVL method experiences considerable variability in positioning accuracy, with some extreme values indicating large errors. These results highlight that while IMU+DVL may perform adequately in some scenarios, its overall reliability is compromised due to the high error spread and instability in other cases.

The IMU+DVL (AE) method exhibits a larger interquartile range (IQR) compared to the other three methods, indicating that its position errors are more widely distributed. The presence of a longer upper whisker and multiple outliers at the higher end suggests that, in some cases, this method produces significantly larger errors, reducing its overall robustness.

The IMU+DVL (CP) method shows a more compact error distribution with a smaller IQR, signifying that its errors are more concentrated and stable. The reduction in outliers compared to IMU+DVL (AE) further confirms its improved

TABLE IV
RMSE AND MAXIMUM POSITION ERRORS (m) FOR DIFFERENT METHODS

Error	INS	INS (AE)	INS (CP)	INS (AE+CP)
δP_N	RMSE	1.3631	0.6769	0.5068
	Max	3.8095	1.7400	1.4903
δP_E	RMSE	2.2202	0.5915	0.4353
	Max	4.5466	1.9836	1.4356
δP_D	RMSE	0.4926	0.3381	0.2326
	Max	1.2873	0.9223	0.5594

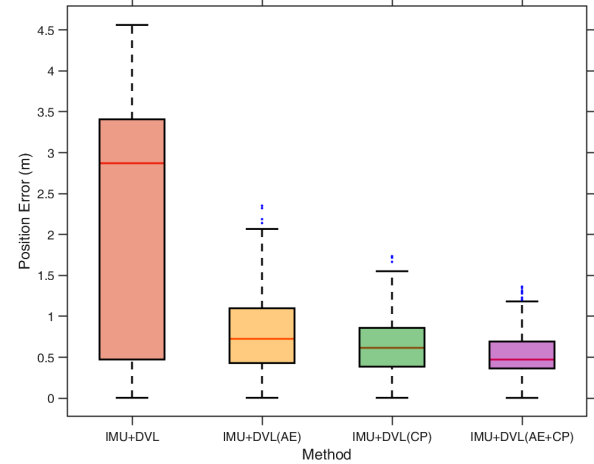


Fig. 10. Position error in the box plot from the experimental results.

consistency, although it still exhibits some degree of variability.

The IMU+DVL (AE+CP) method demonstrates the narrowest IQR, indicating the most consistent performance among the four methods. While outliers are present in this method, they are fewer in number and distributed symmetrically, suggesting that occasional deviations occur but do not significantly impact its overall stability. Additionally, the median position error of IMU+DVL (AE+CP) is lower than that of the other methods, reinforcing its superior accuracy.

Despite the presence of some outliers, IMU+DVL (AE+CP), the method proposed in this paper, remains the most robust and reliable method, exhibiting the smallest error variance while maintaining high accuracy.

C. Comparison and Analysis

A comparison of the simulation and field experimental results shows that the baseline IMU+DVL method exhibits the largest positioning errors, characterized by wide IQRs and pronounced outliers. As illustrated by the box plots in Fig. 6 and Fig. 10, both proposed methods, IMU+DVL (AE) and IMU+DVL (CP), achieve noticeable improvements in positioning accuracy, as evidenced by reduced error dispersion and narrower IQRs. By jointly compensating for attitude-induced velocity projection errors and the associated uncertainty propagation, the combined approach further suppresses extreme errors and yields the most stable and reliable positioning performance among all compared methods.

A notable difference between the simulation and field experimental results is observed in the distribution of outliers. In the simulation results, outliers are mainly concentrated at the lower end of the error distribution, whereas in the field experiments, they are more prominent at the upper end. This discrepancy can be attributed to the idealized modeling conditions in the simulations, where velocity measurement noise, sensor imperfections, and lever arm effects can be more accurately controlled. In contrast, field experiments are subject to unmodeled environmental disturbances and long-term operational effects, which amplify error accumulation in practical scenarios.

More importantly, both simulation and experimental results consistently reveal that, as the underwater vehicle operates over extended periods, attitude estimation errors in the SINS/DVL system gradually accumulate and are directly introduced into the DVL velocity observations through the projection process. The resulting biased velocity measurements further degrade attitude estimation, forming a coupled error propagation mechanism between attitude and velocity states. This phenomenon is clearly reflected in the growing error dispersion and increased outlier magnitude observed in the baseline IMU+DVL results.

After applying the proposed compensation strategies, the divergence of positioning errors is significantly suppressed. In the simulation results shown in Fig. 3, the combined approach achieves a 72.3% improvement in RMSE positioning accuracy and a 74.8% reduction in the maximum positioning error relative to the IMU+DVL method. Similarly, the field experimental results in Fig. 9 demonstrate a 78.3% improvement in the 3D RMSE position error magnitude and a 71.8% reduction in the maximum component-wise position error. The close agreement between simulation and field experiment outcomes confirms that compensating for vehicle attitude-induced errors in both DVL velocity observations and their associated uncertainty propagation is essential for mitigating long-term error accumulation and enhancing the robustness of SINS/DVL loosely coupled navigation systems.

V. CONCLUSION

This paper has investigated the impact of vehicle attitude errors on DVL-based velocity projection and uncertainty modeling in SINS/DVL loosely coupled navigation systems. By jointly considering attitude error effects in both the velocity observation model and the corresponding uncertainty propagation process, a more accurate and statistically consistent navigation framework is established for underwater applications.

Based on the two proposed methodological improvements, extensive simulations and field experiments were conducted to evaluate their effectiveness. Comparative studies were performed to separately assess attitude error compensation in the DVL velocity observation (AE) and attitude-aware uncertainty propagation in the measurement noise model (CP). The results demonstrate that, when applied individually, both approaches can effectively improve navigation accuracy. These findings confirm that velocity projection errors induced by accumulated attitude estimation errors during long-term underwater opera-

tion have a significant impact on the reliability of DVL velocity observations. Moreover, the results further indicate that, as vehicle attitude errors accumulate, not only the projected DVL velocity measurements are affected, but the associated measurement uncertainty is also altered during the projection process, thereby influencing the statistical characteristics of the DVL measurement uncertainty.

Furthermore, when both compensation mechanisms are jointly applied, the proposed approach enables DVL innovations generated in the body coordinate system to be more accurately projected into the navigation coordinate system for loosely coupled fusion. Field experimental results show that, compared with the uncompensated IMU+DVL solution, the proposed method achieves a 78.3% improvement in position RMSE and a 71.8% reduction in the maximum component-wise position error, effectively mitigating the adverse effects of attitude error accumulation during prolonged navigation. This combined strategy provides a more robust data fusion scheme for SINS/DVL loosely coupled navigation systems in practical engineering applications.

Due to limitations of the experimental environment and testing platform, absolute ground truth data for the underwater vehicle were not available in this study, as such information is typically obtained using long baseline (LBL) systems or equivalent reference equipment. Future work will therefore focus on conducting more comprehensive experimental validations by incorporating high-precision reference systems, such as PHINS, to further assess the performance and robustness of the proposed method under diverse operational conditions.

REFERENCES

- [1] D. Terracciano, L. Bazzarello, A. Caiti, R. Costanzi, and V. Manzari, “Marine robots for underwater surveillance,” *Current Robotics Reports*, vol. 1, no. 4, pp. 159–167, 2020.
- [2] A. D. Rogers and E. Ramirez-Llodra, “Deep-sea exploration of marine ecosystems – knowledge and solutions for marine biodiversity,” *The International Hydrographic Review*, vol. 30, no. 1, pp. 10–37, 2024.
- [3] E. Shields and M. Imtiaz, “A review of recent advancements in sensors employed in unmanned underwater vehicles,” *Engineering*, Preprint, 2023.
- [4] F. Ponzini, C. Fruzzetti, and N. Sabatino, “Real-time critical marine infrastructure multi-sensor surveillance via a constrained stochastic coverage algorithm,” *Conference Proceedings of iSCSS*, 2024.
- [5] G. Ioannou, N. Forti, L. M. Millefiori, S. Carniel, A. Renga, G. Tomasichio, S. Binda, and P. Braca, “Underwater inspection and monitoring: Technologies for autonomous operations,” *IEEE Aerospace and Electronic Systems Magazine*, vol. 39, no. 5, pp. 4–16, 2024.
- [6] C. M. Duarte, *Ocean - The Secret of Planet Earth*. Springer Nature, 2024.
- [7] D. Ma, T. Ma, Y. Li, and Q. Miao, “Constrained zonotope terrain-aided navigation method for long-range autonomous underwater vehicles,” *IEEE/ASME Transactions on Mechatronics*, pp. 1–13, 2025.
- [8] L. Paull, S. Saeedi, M. Seto, and H. Li, “AUV Navigation and Localization: A Review,” *IEEE Journal of Oceanic Engineering*, vol. 39, no. 1, pp. 131–149, 2014.
- [9] P. Chen, Y. Li, Y. Su, X. Chen, and Y. Jiang, “Review of AUV Underwater Terrain Matching Navigation,” *Journal of Navigation*, vol. 68, no. 6, pp. 1155–1172, 2015.
- [10] B. Zhang, D. Ji, S. Liu, X. Zhu, and W. Xu, “Autonomous Underwater Vehicle navigation: A review,” *Ocean Engineering*, vol. 273, p. 113861, 2023.
- [11] Y. Wang, R. Hu, P. Du, W. Yang, Y. Chen, and S. H. Huang, “One-Way-Travel-Time Hybrid Baseline Navigation for Micro Autonomous Underwater Vehicles,” *IEEE Journal of Oceanic Engineering*, pp. 1–17, 2025.

[12] H. Li, Z. Liu, J. Huang, X. An, and Y. Chen, “An Improved ESO-based Line-of-Sight guidance law for path following of underactuated Autonomous Underwater Helicopter with nonlinear tracking differentiator and anti-saturation controller,” *Ocean Engineering*, vol. 322, p. 120456, 2025.

[13] F. Maurelli, S. Krupiński, X. Xiang, and Y. Petillot, “AUV localisation: A review of passive and active techniques,” *International Journal of Intelligent Robotics and Applications*, vol. 6, no. 2, pp. 246–269, 2022.

[14] D. Engelsman and I. Klein, “Information-Aided Inertial Navigation: A Review,” *IEEE Transactions on Instrumentation and Measurement*, vol. 72, pp. 1–18, 2023.

[15] Q. Luo, X. Yan, C. Wang, Y. Shao, Z. Zhou, J. Li, C. Hu, C. Wang, and J. Ding, “A SINS/DVL/USBL integrated navigation and positioning IoT system with multiple sources fusion and federated Kalman filter,” *Journal of Cloud Computing*, vol. 11, no. 1, p. 18, 2022.

[16] X. Du, X. Pang, F. Guan, J. Hu, and W. Zhang, “A novel multi-source navigation algorithm based on factor graph in complex underwater environments of polar regions,” *Ocean Engineering*, vol. 301, p. 117516, 2024.

[17] H. Hongyang, Z. Bing, T. Ge, M. Ning, Y. Yanting, and Y. Yun, “Robust adaptive SINS/DVL initial alignment method based on variational Bayesian information filter,” *IEEE Sensors Journal*, pp. 1–1, 2024.

[18] P. Liu, B. Wang, Z. Deng, and M. Fu, “A Correction Method for DVL Measurement Errors by Attitude Dynamics,” *IEEE Sensors Journal*, vol. 17, no. 14, pp. 4628–4638, 2017.

[19] J. Li, M. Gu, T. Zhu, Z. Wang, Z. Zhang, and G. Han, “Research on Error Correction Technology in Underwater SINS/DVL Integrated Positioning and Navigation,” *Sensors*, vol. 23, no. 10, p. 4700, 2023.

[20] D. Wang, X. Xu, and L. Hou, “An Improved Adaptive Kalman Filter for Underwater SINS/DVL System,” *Mathematical Problems in Engineering*, vol. 2020, pp. 1–14, 2020.

[21] Y. Huang, X. Liu, Z. Wang, and X. Wu, “Estimation of constant ocean current velocity based on SINS/DVL integrated navigation with an augmented observable quantities filter,” *Ocean Engineering*, vol. 284, p. 115288, 2023.

[22] P. Gao, F. Qin, K. Li, L. Chang, L. Qian, and T. Zhu, “The Euler angle error model based on attitude error of body frame in ECEF frame,” *IEEE Sensors Journal*, pp. 1–1, 2025.

[23] Y. Yao, Y. Shen, X. Xu, K. Deng, and X. Xu, “A Modified Smoothing Scheme for Water Current-Aided SINS/DVL Integration System,” *IEEE Sensors Journal*, vol. 23, no. 21, pp. 26366–26374, 2023.

[24] D. Wang, X. Xu, Y. Yao, T. Zhang, and Y. Zhu, “A Novel SINS/DVL Tightly Integrated Navigation Method for Complex Environment,” *IEEE Transactions on Instrumentation and Measurement*, vol. 69, no. 7, pp. 5183–5196, 2020.

[25] D. Wang, B. Wang, H. Huang, B. Xu, and H. Zhang, “A Novel SINS/DVL Integrated Navigation Method Based on Different Track Models for Complex Environment,” *IEEE Transactions on Instrumentation and Measurement*, vol. 73, pp. 1–12, 2024.

[26] N. Cohen and I. Klein, “Seamless Underwater Navigation with Limited Doppler Velocity Log Measurements,” *IEEE Transactions on Intelligent Vehicles*, pp. 1–12, 2024.

[27] S. Thrun, W. Burgard, and D. Fox, *Probabilistic Robotics*, 1st ed. Cambridge, Mass: The MIT Press, 2005.

[28] B. D. O. Anderson and J. B. Moore, *Optimal Filtering*. Mineola, NY: Dover Publications, 2005.

[29] P. D. Groves, *Principles of GNSS, Inertial, and Multisensor Integrated Navigation Systems, Second Edition*. Artech House, 2013.

[30] X. Niu, Q. Zhang, L. Gong, C. Liu, H. Zhang, C. Shi, J. Wang, and M. Coleman, “Development and evaluation of GNSS/INS data processing software for position and orientation systems,” *Survey Review*, vol. 47, no. 341, pp. 87–98, 2015.

[31] J. Huang, H. Li, Z. Liu, Z. Wang, Y. Wang, and Y. Chen, “GNSS-aided installation error compensation for DVL/INS integrated navigation system using error-state Kalman filter,” *Measurement*, vol. 242, p. 116224, 2025.

[32] P. A. Miller, J. A. Farrell, Y. Zhao, and V. Djapic, “Autonomous Underwater Vehicle Navigation,” *IEEE Journal of Oceanic Engineering*, vol. 35, no. 3, pp. 663–678, 2010.

[33] T. S. Shores, *Applied Linear Algebra and Matrix Analysis*, ser. Undergraduate Texts in Mathematics. Springer, 2007.